Synergistic Effects of Doping Aluminum and Poly (Vinyl Alcohol) on ZnO Photocatalyst for Catalytic Degradation of Methyl Orange under Sunlight

Yemane Amare[1], Tesfay Welderfael*[2], Om Prakash Yadav[3] and Taame Abraha Berhe[4]

[1]Chemistry Department, College of Natural and Computational Sciences, Aksum University, Aksum, P.O Box: 1010, Ethiopia (yem21amare@gmail.com; ORCID: https://orcid.org/0009-0003-7951-2382).

[2]Chemistry Department, College of Natural and Computational Sciences, Aksum University, Aksum, P.O. Box: 1010, Ethiopia (*weltesf@gmail.com; ORCID: https://orcid.org/0009-0002-6373-5074).

[3]Chemistry Department, CCS Haryana Agricultural University, Hisar-125004, India (yadavop02@yahoo.com; ORCID: https://orcid.org/0000-0001-5380-02960).

[4]Chemistry Department, College of Natural and Computational Sciences, Adigrat University, Adigrat, P.O. Box: 50, Ethiopia (taame.abraha@adu.edu.et; ORCID: https://orcid.org/0000-0002-2541-6315).

ABSTRACT

Photocatalytic wastewater treatment using suitable semiconductor nanomaterials as photocatalysts is currently a promising alternative for addressing urgent environmental issues related to various persistent pollutants, such as dyes and pesticides. To this end, ZnO, Al-modified ZnO and ZnO/PVA nanoscale photocatalysts were synthesized using co-precipitation methods. UV-Vis, XRD, SEM and FTIR methods were then used to characterize these nanomaterials. Additionally, the photocatalysts' catalytic activity was determined by evaluating their ability to remove methyl orange (MO) dye from an aqueous medium using sunlight. To enhance the efficiency of the photocatalytic process, ZnO was doped with aluminum, after which a composite was formed with polyvinyl alcohol (PVA). This process is responsible for both narrowing the band gap and hindering the recombination of charge carriers, thereby improving the activity of the ZnO nanocomposite when exposed to sunlight. The extent of MO removal was as follows: (Al- modified ZnO /PVA) > (Al-modified ZnO) > (ZnO/PVA) > (pure ZnO). The results showed that doping ZnO with aluminum and combining it with PVA enhanced the catalytic activity. Using Al- modified ZnO /PVA as a catalyst achieved 83.7% MO removal in 90 minutes. The Al- modified ZnO composite with PVA exhibited a synergistic effect. This could inform strategies for the removal of organic dyes. Furthermore, these results suggest that doping is an alternative mechanism for enhancing the removal of organic dyes, such as MO, under sunlight, thereby helping to green the environment.

Keywords: Photocatalytic, Degradation, Methyl orange, Nanostructures, Al-modified ZnO/PVA.

1. INTRODUCTION

Dyes are organic pollutants that impart color to substances, including textiles, fibers, leather, hair and plastic materials, either in solution or in dispersion (Welderfael et al., 2013). Humans have been familiar with dyes since prehistoric times, using them to color fabrics, mostly derived from natural plants (Kavitha et al., 2025). Yadav et al. (2023) have described the fundamental aspects of dyes and natural pigments, including their chemical constituents and classification, and the methods of production and dyeing mechanisms that are responsible for the formation of diverse colors and their future prospects. Artificial dyes are characterized by their ability to impart a fixed color to a substance and resist fading when exposed to light,

Submitted: 21st February 2025 ***Accepted: 9th February 2026*** ***Published: 2nd May 2026***

washing or chemicals such as acids and bases (Kavitha et al., 2025). Of the more than ten thousand dyes used in the textile manufacturing industry, nearly 70% are azo dyes, which are extremely toxic, carcinogenic and non-biodegradable (Bhapkar et al., 2023). The main source of color discharge into the environment is the partial exhaustion of dyes onto textile fibers during the dyeing process. Therefore, there is a need to remove residual dyes and other toxic pollutants from industrial effluents. This is because access to clean water is essential for all living species (Hassaan and El Nemr, 2017).

In recent decades, photocatalytic wastewater treatment using suitable semiconductor nanomaterials has emerged as a promising alternative for addressing the pressing environmental challenge posed by recalcitrant pollutants such as toxic dyes and pesticides. In the heterogeneous photocatalytic process involving metal oxide semiconductor nanoparticles, organic dyes in wastewater are completely degraded into harmless products, such as inorganic minerals, water, and CO_2 (Subramani and Senthilnathan, 2019). ZnO semiconductor nanomaterials have been widely used to decolorize wastewater contaminated with dyes. ZnO is a well-known n-type semiconductor and a member of the (II-VI) metal oxide family that occurs naturally as the mineral zincite. With a binding energy of 60 MeV and a band gap of 3.4 eV, ZnO is an encouraging semiconductor for use in electronics, optics, solar cells, transistors, photodetectors, and gas sensors. There are three polymorphs of the ZnO crystalline structure: wurtzite, zincblende, and rock salt. The wurtzite structure is the most thermodynamically stable phase. Consequently, researchers have paid more attention to ZnO in the wurtzite structure (Lam et al., 2012; Reynolds et al., 1998; Welderfael et al., 2016). Furthermore, metal oxides such as ZnO and TiO_2 nanocrystals are promising materials for use in solar cells, photoelectron-chemical water splitting, and degrading organic contaminants. Generating hydrogen fuel via solar water splitting is an important area of research interest due to the environmentally friendly, and low-cost nature of ZnO. However, the application of ZnO photocatalysts presents advantageous opportunities as well as challenges that limit their suitability for various purposes.

The main challenge is its large band gap, which reduces responsiveness to visible light absorption and increases electron-hole recombination and photo-corrosion in acidic or basic solutions (Arunachalam and Al Mayouf, 2019). Methods to improve the photocatalytic activity of ZnO under visible radiation include increasing the specific surface area, generating defect sites, and surface modification with suitable metals or nonmetals. Joseph et al. (2020) have reported that doping an iron oxide nonporous structure with aluminum reduces its band gap. Polyvinyl alcohol (PVA) is commonly used as an encapsulant or component of

composite photocatalysts to enhance the efficiency of nanocomposite photocatalysts (Agorku et al., 2023; Faeq et al., 2023). Methyl orange (MO), a popular pH indicator used in titration, exhibits a red color in an acidic medium (pH < 7) and a yellow color in an alkaline medium (pH > 7). Ingesting drinking water contaminated with MO can lead to gastrointestinal irritation, nausea, vomiting, diarrhea, and respiratory tract irritation. This study presented the synergistic effect of aluminum doping in combination with PVA in ZnO to improve the photocatalytic degradation of MO under sunlight as a new approach. The extent of MO removal was found to be in the following order: Al- modified ZnO/PVA > Al- modified ZnO > ZnO/PVA > pure ZnO. The Al- modified ZnO composite with PVA achieved 83.7% MO degradation in 90 minutes. The result would present new findings on how Al doping (which typically alters electronic properties such as narrowing band gap) and PVA incorporation (which might affect morphology and surface area) together help to achieve a performance higher than using either dopant alone, specifically for the degradation of Methyl Orange (MO) under sunlight. The simultaneous use and the observed combined effect might be a new approach in this field. This has implications for green catalysis technology in sustainable wastewater cleaning and conversion, as well as for achieving sustainable development goals relating to green economic development.

2. EXPERIMENTAL SECTION

2.1. Chemicals

The chemicals used are Sodium hydroxide (NaOH, MW: 39.997 g/mol, Sigma Aldrich, 97%, India), Aluminum chloride ($AlCl_3$, MW: 133.34 g/mol, Sigma Aldrich, 97%, India), Zinc nitrate hexahydrate ($Zn(NO_3)_2.6H_2O$, MW: 297.49 g/mol, Sigma Aldrich, 98%, India); Methyl orange ($C_{14}H_{14}N_3NaO_3S$, MW: 327.33 g/mol, Sigma Aldrich, 98%, India) and Polyvinyl alcohol) (PVA), MW: 89,000-98,000, Sigma Aldrich, 97%, India).

2.2. Method

2.2.1. Synthesis of ZnO Nanoparticles

Typically, 100 mL of a 0.05 M zinc nitrate hexahydrate ($Zn(NO_3)_2 \cdot 6H_2O$) solution was slowly added to 100 mL of a 0.1 M sodium hydroxide (NaOH) solution in a 400 mL Pyrex glass beaker. The reaction mixture was stirred continuously with a magnetic stirrer for 25 minutes. The resulting white, gelatinous precipitate was washed three times with deionized water and then dried in an oven at 80°C. Finally, the product was calcined at 400°C in a ceramic crucible to produce ZnO powder (Kumar, 2016).

2.2.2. Synthesis of Al-modified ZnO Nanoparticles

A 400-ml Pyrex glass beaker containing 100 ml of deionized water was used to mix zinc nitrate hexahydrate and aluminum chloride at a molar ratio of 100:3. The mixture was stirred magnetically for half an hour to produce a clear solution. Then, a 0.1 M NaOH aqueous solution was added dropwise at 60 °C with continuous stirring, producing white precipitates. The product was filtered and repeatedly washed with deionized water until the filtrate was neutral (pH 7.0). Finally, the product was dried in an oven at 80°C for four hours and calcined at 400°C to obtain aluminum-modified zinc oxide powder (Giovannelli et al., 2014).

2.2.3. Synthesis of ZnO/PVA Nanocomposites

50 ml of deionized water was used to dissolve 10g of PVA powder by slow heating on a hot plate for 20 minutes using magnetic stirring. The resulted zinc oxide powder was mixed with PVA solution to achieve a ZnO: PVA ratio of 1:2. The mixture was stirred continuously until a uniform dispersion was obtained. The mixture was left to dry overnight in a dust-free environment at ambient temperature, resulting in ZnO/PVA nanocomposite powder.

2.2.4. Synthesis of Al-modified ZnO/PVA Nanocomposite

Typically, 100 mL of deionized water was placed in a 400 mL Pyrex glass beaker and used to dissolve 10 g of PVA powder. The mixture was magnetically stirred and gently heated for 20 minutes to obtain the PVA aqueous solution. Then, the Al-modified ZnO powder was added to the aqueous PVA solution at 1:2 ratios. After stirring for an additional 20 minutes, a uniform aqueous dispersion was produced. Finally, the mixture was dried in a dust-free chamber at room temperature to produce the Al-modified ZnO/PVA composite powder.

2.3. Characterization Techniques

2.3.1. X-Ray diffraction Study

X-ray diffraction (Shimadzu XRD 600) was used to record the diffraction pattern of a 10 mg powder sample. The XRD used Cu/Kα radiation at a wavelength of 1.5406 Å, operating at a voltage of 40 kV and a current of 40 mA. The XRD pattern was recorded over the 2θ range: 3° to 70° using a scan rate of 2°/min at 25°C and under constant operational conditions.

2.3.2. UV-Visible Absorption Measurements

Typically, the absorption spectra of 10 mg powder dispersed in 20 ml deionized water were recorded using a single-beam spectrophotometer (Mettler Toledo) scanning over 200-800 nm. The Tauc's plot used to obtain the band gap of the powder based on equation (1)(Tauc et al., 1970).

$$\alpha h\nu = K\sqrt{(h\nu - Eg)} \qquad (1)$$

Where, Eg = optical band gap energy; hv = incident photon energy; K = energy independent constant; and α = absorption coefficient.

2.3.3. FTIR Analysis Study

A small amount of the sample powder was mixed with KBr and ground into a thin pellet. The pellet was placed in the infrared path and the spectrum was recorded using a Jasco Instruments model 100 FTIR spectrometer (from Japan) at a resolution of 2 cm^{-1} over the frequency range of 500 to 4000 cm^{-1}.

2.4. Photocatalytic Degradation of Methyl Orange

The batch method was used to study the photocatalytic degradation of the methyl orange (MO) dye. As-synthesized ZnO, Al-modified ZnO, ZnO/PVA, and Al-modified ZnO/PVA powders were used as catalysts. Typically, a 400 ml Pyrex glass beaker containing 100 ml of a 15 mg/L MO aqueous solution was used to dissolve 30 mg of catalyst powder. The beaker containing the reaction mixture was kept in the dark for 30 minutes to reach sorption/desorption equilibrium. Then, it was exposed directly to sunlight on cloudless days from 11 AM to 1 PM (Fig 1) using sunlight intensity conditions of power 6W using a magnetic stirrer and a spectrophotometer (UV-2450, Shimadzu) operated under 30°C temperature during stirring and the whole experiment. Air was continuously bubbled through the reaction mixture, which also served to stir it. Six milliliters of the reaction mixture were collected at time intervals using a 10-milliliter pipette. The mixture was filtered using Whatman paper, and the absorbance of the clear filtrate was recorded at 460 nm. The % degradation of MO was calculated using equation 2 (Lee et al., 2015).

$$\% \text{ Degradation} = \frac{A0 - At}{A0} x100 \qquad (2)$$

Where, t = time; A_t = absorbance values at the final stage; A_0 = absorbance values at the initial stage (t=0).

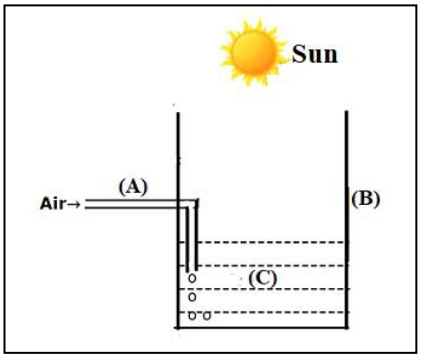

Figure 1. The arrangement for photocatalytic degradation of MO under the exposure of sunlight. (A) Stands for tube for air purging; (B) stands for 400 ml Pyrex glass beaker and (C) stands for reaction mixture.

3. RESULTS AND DISCUSSION

3.1. Structure Property Characterization

Figure 2a shows the XRD spectra of the as-prepared ZnO, Al-modified ZnO, ZnO/PVA, and Al-modified ZnO/PVA powders. The sharp diffraction peaks observed for the ZnO powder at 2θ = 31.766º, 34.418º, 36.251º, 47.535º, 56.591º, 62.857º and 67.90º are due to reflections from the (100), (002), (101), (102), (110), (103), and (112) crystal planes, respectively. These peaks confirm the formation of a pure, single-crystal hexagonal ZnO structure, as evidenced by the matching JCPDS card 36-1451 diffraction data. Additionally, the well-separated diffraction peaks in the XRD pattern indicate the formation of an ultra-fine ZnO crystal structure.

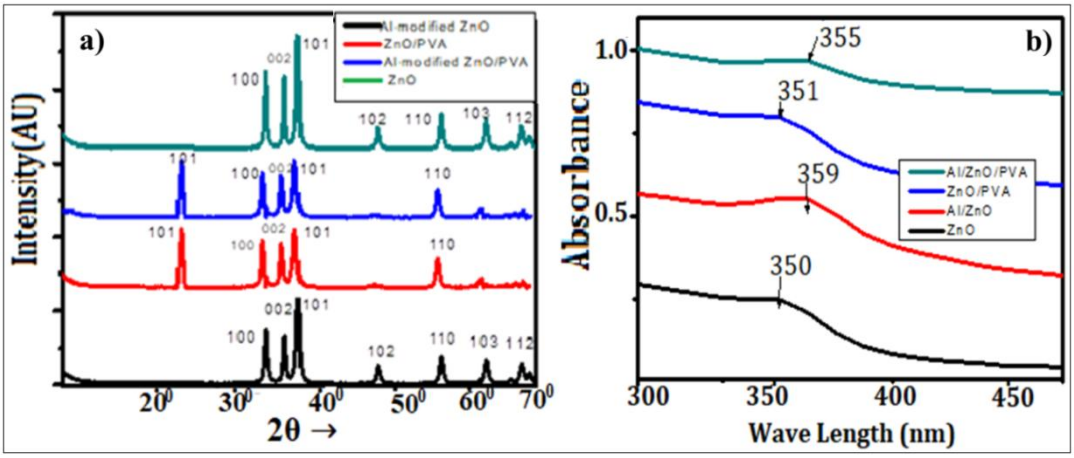

Figure 2. Crystal structure and absorption spectra: a) The XRD patterns of ZnO, Al-modified,ZnO/PVA and Al-modified ZnO/PVANanocomposites b) UV-Visible absorption spectrum of ZnO, Al-modified ZnO, ZnO/PVA and Al-modified ZnO/PVA.

The observed 2θ values for the Al-modified ZnO powder are 32.172°, 34.604°, 36.495°, 47.568°, 56.780°, 62.726° and 67.534°, are due to reflections from the (100), (002), (101), (102), (110), (103) and (112) suggesting that the hexagonal ZnO crystal structure remains intact even upon aluminum doping.

The observed 2θ values for the PVA/ZnO are 31.73°, 34.54°, 36.33° and 56.41°, are because of the reflections from (100), (002), (101), and (110) indicating that the hexagonal ZnO crystal structure diminishes partially upon PVA addition. Moreover, the observed 2θ values for the Al-modified ZnO/PVA are 31.84°, 34.74°, 36.45°, and 56.60° are due to reflections from the (100), (002), (101) and (110) showing that the hexagonal ZnO crystal structure reduces some peaks upon Al and PVA co-modification. The XRD patterns of the ZnO/PVA and Al-modified ZnO/PVA nanocomposite powders are almost identical, with two unique features compared to the XRD pattern of pure ZnO: (1) the appearance of an additional diffraction peak at θ/2 = 18.1°, due to reflection from the (101) plane of the PVA

crystal and (2) the diminishing intensity of the diffraction peaks, which indicates their poor crystalline structure.

The crystallite size of the as-synthesized nanomaterial was calculated using the Scherer formula (Du et al., 2006) represented by equation 3.

$$D = 0.9\frac{\lambda}{\beta \cos\theta} \qquad (3)$$

Where, β = full width at half maximum (FWHM); θ = Bragg's angle; Factor of 0.9 is the Scherer constant; λ = X-ray wavelength (1.5406 Å); and D = crystallite size in nm.

Therefore, the average crystal sizes of the ZnO, Al-modified ZnO, ZnO/PVA and Al-modified ZnO/PVA nanostructures are 45.9, 41.8, 35.66 and 35.18 nm, respectively. Due to the addition of Al and PVA the crystal sizes of ZnO was reduced. The crystallite size of the Al-modified ZnO/PVA nanocomposite powder (35.18 nm), as calculated using the Scherer formula, was slightly smaller than that of the ZnO/PVA nanocomposite powder (35.62 nm).

According to Ahmad et al. (2013), the appearance of well-separated diffraction peaks in the XRD pattern indicates the formation of an ultra-fine crystal structure of ZnO. The slight drifting of the peaks to higher 2θ can be attributed to the entrapment of smaller Al^{3+} ions (ionic radius 0.050 nm) within the interstitial positions of the ZnO crystal lattice (ionic radius of Zn^{2+} 0.074 nm). The Al-O bond length is shorter than the Zn-O bond length, resulting in diminished unit cell dimensions of Al-modified ZnO. Thus, doping Al^{3+} ions into ZnO slightly changes the crystal lattice as well as the d-spacing within the constituent ions. The diminished size of the observed diffraction peaks in the Al-modified ZnO XRD pattern indicates poor crystal quality. The XRD patterns of ZnO/PVA and Al-modified ZnO/PVA nanocomposite powders are almost identical, with two unique features compared to the XRD pattern of pure ZnO: the appearance of an additional diffraction peak at 2θ = 19.52°, due to reflection from the (101) plane of the PVA crystal; and diminished peak intensity, indicating poor crystal structure. The crystallite size of Al-modified ZnO/PVA (35.18 nm), obtained using the Scherer formula, was slightly smaller than that of ZnO/PVA (35.62 nm).

Furthermore, UV-Vis spectroscopy reveals that the composite powders of ZnO, Al-modified ZnO, ZnO/PVA, and Al-modified ZnO/PVA exhibit broad absorption bands at 350, 359, 351, and 355 nm, respectively. Al modified in ZnO and compositing PVA with ZnO both result in red-shifting of the absorption peak due to band gap narrowing (Rahman et al., 2019; Yung et al, 2009). Additionally, UV-visible spectroscopy reveals broad absorption bands at 350 nm, 359 nm, 351 nm, and 355 nm for ZnO, Al-modified ZnO, ZnO/PVA, and Al-modified ZnO/PVA composite powders (Fig 2b). Al doping in ZnO and compositing

PVA with ZnO both result in red-shifting of the absorption peak due to band gap narrowing. It clearly shows that doping Al into ZnO and compositing PVA with ZnO decrease band gap energies synergistically. Furthermore, doping Al into ZnO and compositing PVA with ZnO introduces new energy states within ZnO's two electronic bands. Consequently, effective band gap narrowing facilitates electron crossing (Rtimi et al., 2022) and improves the photocatalyst's catalytic activity in visible light exposure (Fu et al., 2011).

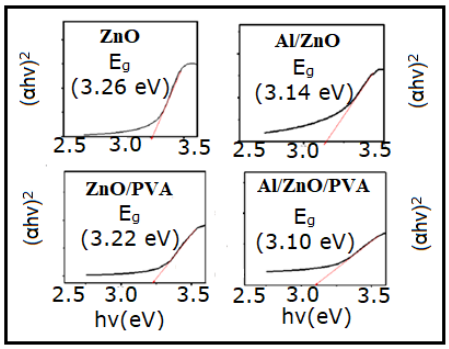

Figure 3. Plots of $(\alpha hv)^2$ versus hv, and the derived optical band gap energy (E_g) of ZnO nanoparticles, Al-modified ZnO, ZnO/PVA nanocomposite and Al-Modified ZnO/PVA nanocomposite.

Figure 3 shows the absorption band edges of pure ZnO, ZnO/PVA, Al-modified ZnO, and Al-modified ZnO/PVA composite powders to calculate the band gap of each semiconductor photocatalyst. The tangent line drawn from the inflection point of the plot to the point of intersection with the horizontal energy (hv) axis gives the band gap energy (Eg) in electron volts. The band gaps for pure ZnO, ZnO/PVA, Al-modified ZnO, and Al-modified ZnO/PVA composite powders were found to be 3.26 eV, 3.22 eV, 3.14 eV, and 3.10 eV, respectively. This clearly shows that doping Al into ZnO and compositing PVA with ZnO synergistically decreases the band gap energies.

As shown in figure 4, the FTIR spectra of the pure ZnO, Al-modified ZnO, ZnO/PVA composite, and Al-modified ZnO/PVA composite powders are characterized. The broad bands observed at 3332.6 and 3366.6 cm^{-1} belong to pure ZnO and Al-modified ZnO, respectively, due to the overlap of the symmetric and asymmetric stretching O-H vibrational modes of chemically bonded water molecules.

Additionally, the blue shift (higher frequency absorption) of the Al-modified ZnO band occurs due to Al's greater electron affinity compared to Zn, which enhances the O-H bond energy. The absorption peak appearing at 1650 cm^{-1} is assigned to the bending vibration mode of the bonded water molecules, and the absorption band at 2273 cm^{-1} in the ZnO absorption spectra is due to the stretching vibration of the surface-adsorbed carbon dioxide. The single strong absorption peak at 696 cm^{-1} and the two vibration bands between 500 and

900 cm^{-1} represent the vibrational modes of the Zn–O and Al–O bonds, respectively. The Al-modified ZnO sample displays two peaks between 700 and 902 cm^{-1} that confirm the presence of the Al-O bond.

Figure 4. FTIR Spectra of synthesized ZnO nanoparticles, Al-modified ZnO nanoparticles, ZnO/PVA nanocomposite and Al-Modified ZnO/PVA nanocomposite Powders.

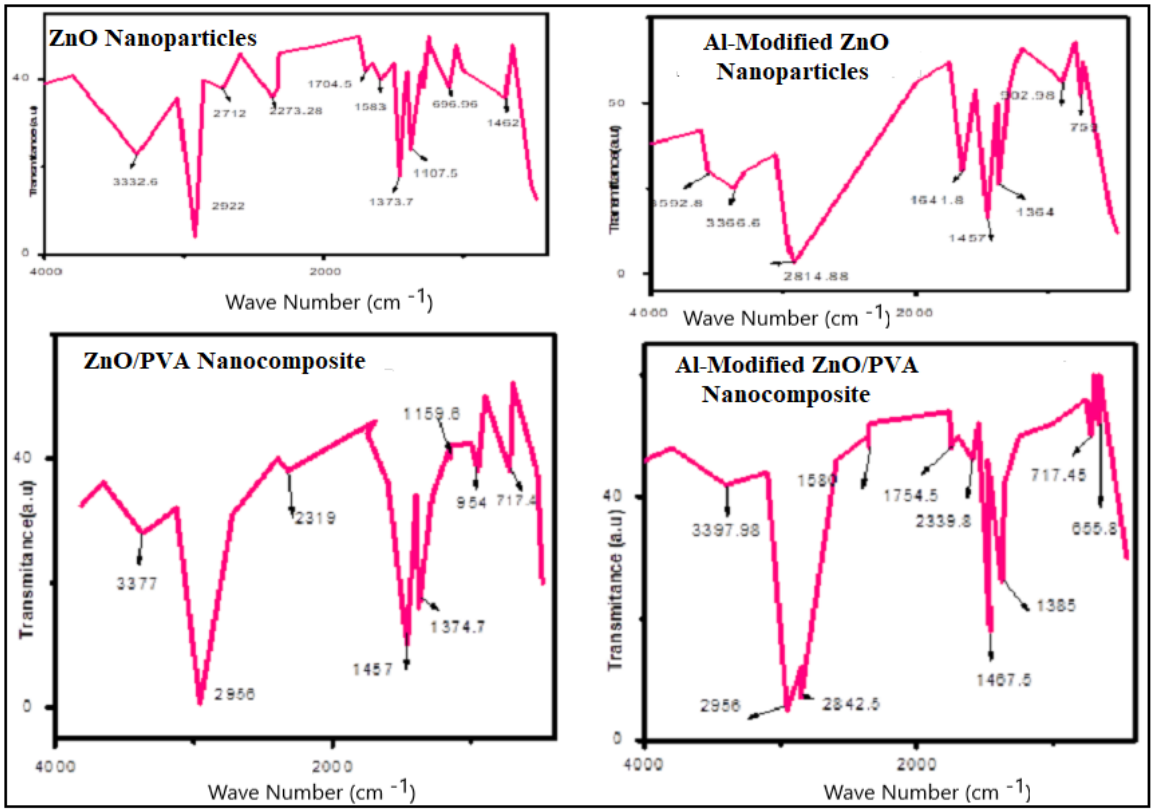

In the FTIR spectra of ZnO/PVA and Al-modified ZnO/PVA, the strong band at 2956 cm^{-1}) is attributed to the asymmetric stretching of CH_2. The band observed at 1754 cm^{-1} is due to the stretching vibration of C=O in the PVA molecules. Furthermore, the bands observed at 1457 and 1375 cm^{-1} in the ZnO/PVA spectra and at 1458 and 1385 cm^{-1} in the Al-modified ZnO/PVA spectra are assigned to the bending and stretching vibrations of CH_2, respectively. Additionally, the absorption bands at 1159.6 and 954 cm^{-1} in the ZnO/PVA spectra are due to C–O stretching and CH_2 rocking vibrations, respectively. Absorptions at 717.4 cm^{-1} in the ZnO/PVA and Al-modified ZnO/PVA spectra arise from out-of-plane OH bending.

The absorption peak appearing at 1650 cm^{-1} is assigned to the bending vibration mode of bonded water molecules, while the absorption band at 2273 cm^{-1} in the ZnO absorption spectra is due to the stretching vibration of surface-adsorbed carbon dioxide. A single strong absorption peak at 696 cm^{-1} and two vibration bands between 500 and 900 cm^{-1} represent the vibrational modes of the Zn–O and Al–O bonds, respectively (Bai et al., 2013). The Al-

modified ZnO sample displays two peaks between 700 and 902 cm^{-1} that confirm the presence of the Al-O bond (Rtimi et al., 2022).

3.2. Morphology Study

Figures 5A & B show the surface morphology of pure ZnO and Al-modified ZnO powder, respectively. The ZnO particles appear to be hexagonal nanorods bound to each other, as shown in figure 5A. However, the Al-modified ZnO powder has larger, randomly oriented, poly-scale morphology and an agglomerated, irregular shape with clear, sharp edges (Fig 5B). This morphological variation when Al is doped into ZnO is due to the replacement of Zn^{2+} with Al^{3+} in the ZnO crystal lattice due to the valence and size differences between the two types of metal atoms.

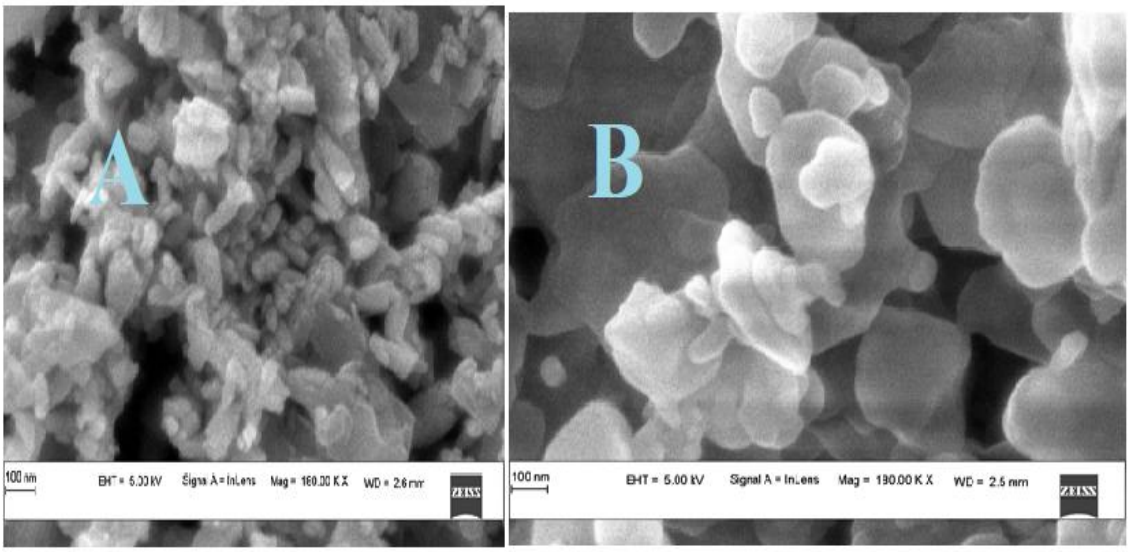

Figure 5. SEM images synthesized (A) ZnO, and (B) Al- modified ZnO powders.

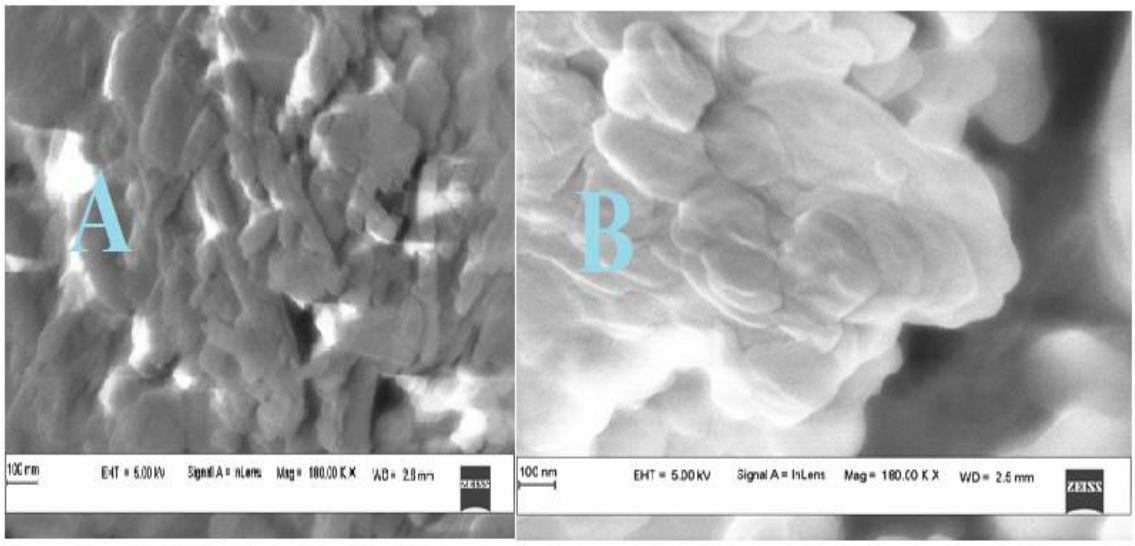

Figure 6. SEM images. (A): ZnO/PVA, and (B): Al- modified ZnO /PVA powders.

Figure 6 (A) & (B) show SEM images of ZnO/PVA and Al-modified ZnO/PVA powder, respectively. The ZnO/PVA nanocomposite appears to be a closely packed, rod-like structure (Fig 6A), whereas the Al-modified ZnO/PVA nanocomposite shows rod-shaped ZnO particles distributed in the PVA matrix (Gutul et al., 2014).

3.3. Degradation of Methyl Orange

The activities of ZnO, Al-modified ZnO, ZnO/PVA, and Al-modified ZnO/PVA powders were studied under sunlight to determine their ability to remove methyl orange (MO) in an aqueous medium. This study recorded the absorbance of the dye solution at λ (max) 460 nm, the dye concentration (C), the log of the initial dye concentration divided by the current dye concentration ($\ln C_0/C$), and the percentage of MO degradation at 30, 60, and 90 minutes. Figure 7 shows the plots of the percentage of MO degradation versus time. Moreover, the Al-modified ZnO/PVA catalyst exhibits the highest photocatalytic activity, causing 83.7% MO degradation at 90 minutes. This is followed by the Al-modified ZnO catalyst (83.3%), the ZnO/PVA catalyst (78.0%), and the ZnO catalyst (76.6%). The higher observed MO removal catalyzed by Al-modified ZnO compared to pure ZnO may be attributed to the change in crystalline phase structure when some Zn^{2+} ions (radius 0.074 nm) are replaced by smaller Al^{3+} ions (radius 0.050 nm).

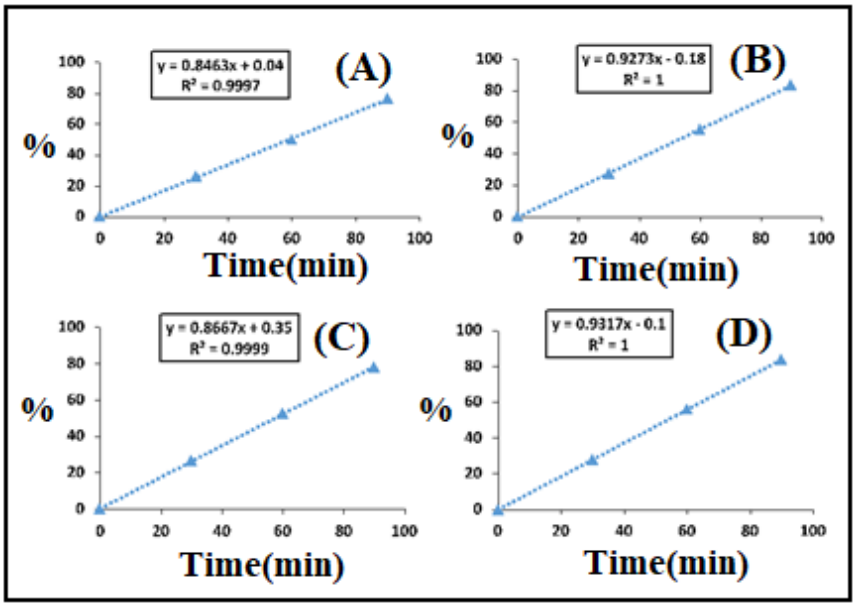

Figure 7. Plots of MO% degradation as a function of reaction time: (A) ZnO, (B) Al- modified ZnO, (C) ZnO/PVA, and (D) Al modified ZnO/PVA [Methyl orange initial concentration(C_0): 15 mg L^{-1}; Catalyst load: 300 mgL^{-1}].

The ZnO/PVA nanocomposite appears to have a closely packed, rod-like structure. In the SEM image of the Al-modified ZnO/PVA nanocomposite, the rod-shaped ZnO particles

are distributed throughout the PVA matrix (Demssie et al., 2020). The higher MO degradation catalyzed by the Al-modified ZnO compared to the pure ZnO may be due to the change in crystalline phase structure that occurs when some of the Zn^{2+} ions (radius 0.074 nm) are replaced by the smaller Al^{3+} ions (radius 0.050 nm). This creates new bands between the conduction and valence bands and minimizes the recombination of charge carriers by trapping them with the doped Al. These effects can result in the generation of more highly oxidizing hydroxyl radicals (˙OH) (Bhapkar et al., 2023). The higher photocatalytic efficiency of the Al-modified ZnO/PVA nanocomposite is due to the high transparency of PVA in visible light (typically, PVA has 99.5% transmittance at 500 nm) and the interaction of metal ions with the hydroxyl groups of PVA molecules, which minimizes the recombination of charge carriers (Bhat and Francis, 2005; Demssie et al., 2020; Bouropoulos et al., 2008).

3.4. Kinetics of Degradation of Methyl Orange

3.4.1. Pseudo First Order Kinetic

During photocatalytic degradation of organic dyes, the Pseudo first order kinetic is given by the equation 4.

$$\ln\left(\frac{C0}{C}\right) = kt \qquad (4)$$

C_0 and C represent the concentrations of the organic dye, such as MO, at the initial stage (t = 0) and at time t, respectively, while k represents the reaction rate constant. Plots of $\log(C_0/C)$ versus time (min) for photocatalytic degradation under sunlight with an initial MO concentration of 15 mg/L and a catalyst load of 300 mg/L are shown in figure 8.

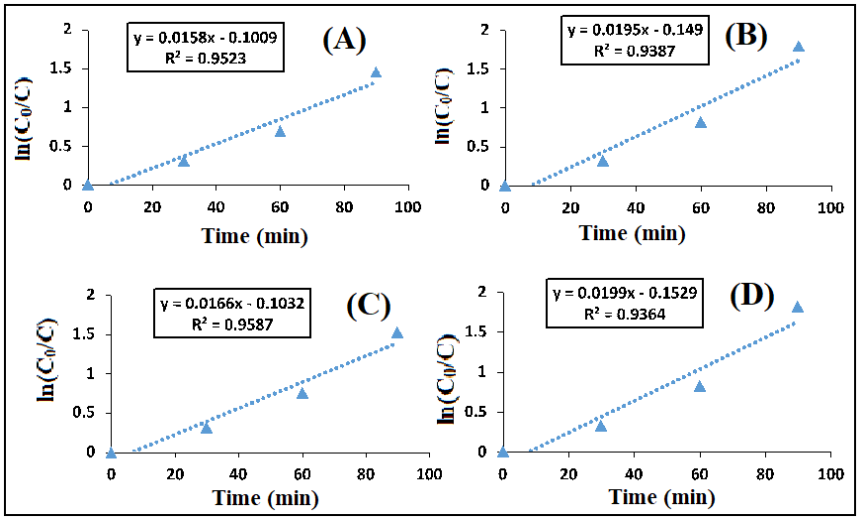

Figure 8. Plots of ln(C_0/C) versus time (min) for photocatalytic degradation methyl orange (MO) dye under sunlight using synthesized catalyst powders; (A) ZnO, (B) Al- modified ZnO, (C) ZnO/PVA, and (D) Al modified ZnO/PVA [MO initial concentration: 15 mg L^{-1}; Catalyst load: 300 mgL^{-1}].

The MO degradation rate constants (k) for different as-synthesized photocatalyst powders were as follows: pure ZnO (k = 1.58 × 10^(−2) min^(−1)), Al-modified ZnO (k = 1.95 × 10^(−2) min^(−1)), ZnO/PVA (k = 1.66 × 10^(−2) min^(−1)), and Al-modified ZnO/PVA (k = 1.99 × 10^(−2) min^(−1)). These results demonstrate that doping Al into ZnO and compositing PVA with ZnO synergistically increase the MO degradation rate, improving it from 76.6% to 83.7% in 90 minutes.

3.5. Proposed Degradation Mechanism

When a semiconductor nanomaterial is exposed to radiation, such as sunlight, it absorbs photons of suitable wavelengths, which excite electrons (e^-) from the valence band (VB) to the conduction band (CB) as proposed in figure 9. This leaves behind a positively charged hole (h^+), according to the proposed degradation mechanism of photocatalysis for this study shown in figure 9. These highly reactive charge carriers (e^- and h^+) cause the degradation of organic material, including MO upon reaching the semiconductor surface. Excited electrons combine with dissolved oxygen at the semiconductor surface to create superoxide radical. Superoxide radicals react with water molecules to generate hydrogen peroxide which readily form hydroxyl radicals. The hole (h^+) at the semiconductor surface interacts with the hydroxyl ($^-$OH) ion to form a hydroxyl radical. These highly oxidizing hydroxyl radicals formed in the above reactions degrade organic pollutants such as MO generating nontoxic products such as H_2O and CO_2 (Ba-Abbad et al., 2013). Additionally, the highly oxidizing holes at the semiconductor surface degrade pollutants such as MO.

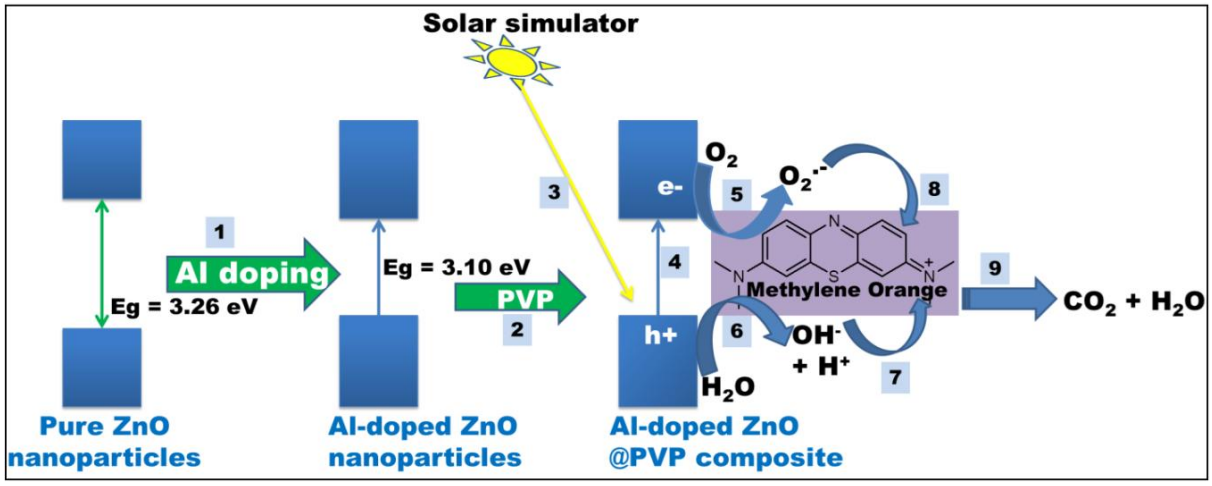

Figure 9. Proposed degradation mechanism of photocatalysis; Al-modified ZnO/PVA composite enabling efficient electrons and holes transfer, resulting in higher photocatalytic activity upon efficient degradation of MO, where 1 = Al-doping, 2 = PVA compositing, 3 = sunlight irradiation, 4 = electron and hole separation, 5 = O_2 trapping electron, 6 = H_2O trapping hole, 7 = OH^- degrading MO, 8 = O_2^- degrading MO and 9 = degradation product

Upon doping aluminum (Al) into the semiconductor zinc oxide (ZnO), the lattice's electrical conductivity and the band structure are altered. This facilitates the transfer of valence electrons to the conduction band due to the narrowing of the band gap (Kalantari et al., 2017; Machrouhi et al., 2023). In the case of a pure semiconductor, also called an intrinsic semiconductor, such as ZnO, charge carriers (e^- and h^+) tend to recombine at the surface, resulting in lower photocatalytic efficiency. However, introducing an impurity, such as Al, into the semiconductor (ZnO) or compositing a polymer, such as PVA, with ZnO to create an extrinsic semiconductor (e.g., Al/ZnO, ZnO/PVA, or Al/ZnO/PVA) can minimize the recombination of charge carriers through trapping. This improves the catalytic efficacy. Figure 3.9 shows the proposed photocatalysis mechanisms under sunlight using Al- modified ZnO/PVA. The results will provide new insights into how aluminum (Al) doping, which typically alters electronic properties such as band gap reduction, and poly vinyl alcohol (PVA) intercalation, which can affect morphology and surface area, work together to achieve higher performance than using a single dopant. This is particularly true in the degradation of methyl orange (MO) under sunlight. Simultaneously using both and observing their combined effect could represent a new approach in this field.

4. CONCLUSION

Nanosized Al-modified ZnO and ZnO were synthesized by co-precipitation methods. ZnO/PVA and Al-modified ZnO/PVA nanocomposites were prepared using the solution casting technique. The Al- modified ZnO/PVA had a smaller size than ZnO/PVA due to the smaller size of the Al^{3+} ions compared to the Zn^{2+} atom. This resulted in a smaller crystal unit cell dimension. The absorption peak patterns observed in the FTIR spectra of the synthesized nanostructures indicated the presence of functional groups, such as O-H, CH_2, and C=O, as well as C–C and Zn–O bonds. Scanning electron microscopy (SEM) images of the synthesized powders revealed that ZnO nanoparticles had hexagonal nanorod-like structures, while Al-modified ZnO nanoparticles were randomly oriented with irregular shapes and clear, sharp surface edges. This morphological variation upon doping Al into ZnO can be attributed to the substitution of Zn^{2+} ions by smaller Al^{3+} ions in the crystal lattice. On the other hand, the ZnO/PVA nanocomposite appeared to be a closely packed, rod-like structure, and the rod-shaped, Al-modified ZnO/PVA nanoparticles were distributed in the PVA matrix. The percent removal of MO after 90 minutes using synthesized powders as catalysts (with an initial MO concentration of 15 mg/L and a catalyst load of 300 mg/L) was found to be: Al-modified ZnO/PVA (83.7%), Al-modified ZnO (83.3%), ZnO/PVA (78.0%), and pure ZnO

(76.6%). The higher observed MO degradation using Al- modified ZnO nano powder compared to pure ZnO could be attributed to the narrowing of the semiconductor's band gap and diminished recombination of charge carriers due to the Al-doping strategy. Furthermore, compositing ZnO with PVA improved the nanocomposite's efficacy due to PVA's high optical transparency in the visible region of sunlight. Consequently, this study suggests that Al-modified ZnO/PVA is useful for removing organic dyes and creating a cleaner, safer environment free of hazardous pollution. The results will provide new insights into how aluminum (Al) doping, which typically alters electronic properties such as band gap reduction, and poly vinyl alcohol (PVA) intercalation, which can affect morphology and surface area, work together to achieve higher performance than using a single dopant. This is particularly true in the degradation of methyl orange (MO) under sunlight. Simultaneously using both and observing their combined effect could represent a new approach in this field. Ultimately, this will help achieve the sustainable development goal of green economic development.

Abbreviations

PVA polyvinyl alcohol
UV-Vis ultraviolet-visible
XRD x-ray diffraction
SEM scanning electron microscopy
FTIR fourier transform infrared
MO methyl orange
MW molecular weight
Eg band gap energy
λmax lambda maximum
C concentration at time t
C_0 initial concentration
e^- Electron
h^+ hole
CB conduction band
VB valence band

5. ACKNOWLEDGEMENTS

It is with great pleasure to acknowledge Aksum University for the financial support of this study. Authors also duly acknowledge the reviewers for their valuable comments.

6. CONFLICT OF INTEREST

There is no conflict of interest.

7. REFERENCE

Agorku, E., Kangmennaa, A., Haruna, M & Opoku, F. 2023. Photocatalytic activity of red emission PVA-$GdVO_4$:Eu nanocomposite towards the degradation of Eosin Y in water. *Sustainable Environment*, **9**, https://doi.org/10.1080/27658511.2023.2266632.

Ahmad, M., Ahmed, E., Zhang, Y., Khalid, N. R., Xu, J., Ullah, M & Hong, Z. 2013. Preparation of highly efficient Al-doped ZnO photocatalyst by combustion synthesis. *Current Applied Physics*, **13(4)**: 697-704, https://doi.org/10.1016/j.cap.2012.11.008.

Arunachalam, P & Al Mayouf, A. M. 2019. Chapter 28 - Photoelectrochemical Water Splitting. In: S. Mohapatra, T. A. Nguyen, & P. Nguyen-Tri (Eds.), *Noble Metal-Metal Oxide Hybrid Nanoparticles* (pp. 585-606): Woodhead Publishing.

Ba-Abbad, M., Kadhum, A., Mohamad, A. B., Takriff, M & Sopian, K. 2013. Visible light photocatalytic activity of Fe3+-doped ZnO nanoparticle prepared via sol–gel technique. *Chemosphere,* **91**, https://doi.org/10.1016/j.chemosphere.2012.12.055.

Bai, X., Wang, L., Zong, R., Lv, Y., Sun, Y & Zhu, Y. 2013. Performance Enhancement of ZnO Photocatalyst via Synergic Effect of Surface Oxygen Defect and Graphene Hybridization. *Langmuir,* **29(9)**: 3097-3105, https://doi.org/10.1021/la4001768.

Bhapkar, A. R., Geetha, M., Jaspal, D., Gheisari, K., Laad, M., Cabibihan, J., Sadasivuni, K. K & Bhame, S. 2023. Aluminium doped ZnO nanostructures for efficient photodegradation of indigo carmine and azo carmine G in solar irradiation. *Applied Nanoscience*, **13(8)**: 5777-5793, https://doi.org/10.1007/s13204-023-02824-3.

Bhat, S. V & Francis, L. 2005. Tuning the bandgap of ZnO by substitution with Mn^{2+}, Co^{2+} and Ni2+. *Solid State Communications*, **135**: 345-347, https://doi.org/10.1016/j.ssc.2005.05.051

Bouropoulos, N., Psarras, G. C., Moustakas, N., Chrissanthopoulos, A & Baskoutas, S. 2008. Optical and dielectric properties of ZnO-PVA nanocomposites. *physica status solidi (a),* **205(8)**: 2033-2037, https://doi.org/10.1002/pssa.200778863.

Demssie, K., Zereffa, E., Murthy, H. C. A & Tullu, A. 2020. Synthesis of ZnO and ZnO/PVA nanocomposite using aqueous Moringa Oleifeira leaf extract template: antibacterial and electrochemical activities. *Reviews on Advanced Materials Science,* **59**: 464-476, https://doi.org/10.1515/rams-2020-0021.

Du, S., Tian, Y., Liu, H & Chen F. 2006. Calcination effects on the properties of gallium-doped zinc oxide powder. *Journal of American Ceramic Soceity*, **89**: 2440-2443.

Faeq, R. I., Jaafar, S. S., Naji, A. M., Mohammed, M. K. A & Nief, O. A. 2023. Increasing the photocatalytic degradation rate of a rGO/PVA nanocomposite decorated with ZnO nanoparticles. *New Journal of Chemistry*, **47(29)**: 13661-13670, https://doi.org/10.1039/D3NJ01521A.

Fu, M., Li, Y., wu, S., Lu, P., Liu, J & Dong, F. 2011. Sol–gel preparation and enhanced photocatalytic performance of Cu-doped ZnO nanoparticles. *Applied Surface Science - APPL SURF SCI, 258*, https://doi.org/10.1016/j.apsusc.2011.10.003.

Giovannelli, F., Ndimba, A., Diaz-Chao, P., Motelica-Heino, M., Raynal, P.-I., Autret, C & Delorme, F. 2014. Synthesis of Al doped ZnO nanoparticles by aqueous coprecipitation. *Powder Technology*, **262**: 203–208, https://doi.org/10.1016/j.powtec.2014.04.065.

Gutul, T., Rusu, E., Condur, N., Ursaki, V & Vlazan, P. 2014. The stretching vibration of Nanocomposites. *Journal of Nanotechnology*, **5**: 402– 406.

Hassaan, M & El Nemr, A. 2017. Health and Environmental Impacts of Dyes: Mini Review. *American Journal of Environmental Science and Engineering*, **1**: 64-67, https://doi.org/10.11648/j.ajese.20170103.11.

Joseph, J. A, Nair, S. B, John, K. A, Babu, S., Shaji, S., Shinoj, V. K & Philip, R. R. 2020. Aluminium doping in iron oxide nanoporous structures to tailor material properties for photocatalytic applications. *J Applied Electrochemistry*, **50**: 81–92, https://doi.org/10.1007/s10800-019-01371-6D.

Kalantari, K., Kalbasi, M., Sohrabi, M & Royaee, S. J. 2017. Enhancing the photocatalytic oxidation of dibenzothiophene using visible light responsive Fe and N co-doped TiO2 nanoparticles. *Ceramics International*, **43(1, Part B)**: 973-981, https://doi.org/10.1016/j.ceramint.2016.10.028.

Kavitha, G., Govindhan, M & Premkumar, S. 2025. Dye pollution and its implications for human health, aquatic ecosystems, and sustainable wastewater treatment: A comprehensive review. *Journal of Water Process Engineering*, **80**: 109071, https://doi.org/10.1016/j.jwpe.2025.109071.

Kumar, P. V. 2016. Synthesis and characterization of ZnO nanoparticles by co-precipitation method at room temperature. *J. Chemical and Pharmaceutical Research*, **8**: 624-628.

Lam, S.-M., Sin, J.-C., Abdullah, A. Z & Mohamed, A. R. 2012. Degradation of wastewaters containing organic dyes photocatalysed by zinc oxide: a review. *Desalination and Water Treatment,* **41(1)**: 131-169, https://doi.org/10.1080/19443994.2012.664698.

Lee, H., Kim, J., Park, S., Hong, S & Lee, G. D. 2015. Degradation kinetics for photocatalytic reaction of methyl orange over Al-doped ZnO nanoparticles. *Journal of Industrial and Engg Chem.,* **25**: 199-206, https://doi.org/10.1016/j.jiec.2014.10.035.

Machrouhi, A., Khiar, H., Elhalil, A., Sadiq, M., Abdennouri, M & Barka, N. 2023. Synthesis, characterization, and photocatalytic degradation of anionic dyes using a novel ZnO/activated carbon composite. *Watershed Ecology and the Environment,* **5**: 80-87, https://doi.org/10.1016/j.wsee.2022.12.001.

Rahman Khan, M. M., Pal, S., Hoque, M. M., Alam, M. R., Younus, M & Kobayashi, H. 2019. Simple Fabrication of PVA-ZnS Composite Films with Superior Photocatalytic Performance: Enhanced Luminescence Property, Morphology, and Thermal Stability. *ACS Omega*, **4(4)**: 6144-6153, https://doi.org/10.1021/acsomega.8b02807.

Reynolds, D. C., Look, D. C., Jogai, B., Litton, C. W., Collins, T. C., Harsch, W & Cantwell, G. 1998. Neutral-donor--bound-exciton complexes in ZnO crystals. *Physical Review B,* **57(19)**: 12151-12155, https://doi.org/10.1103/PhysRevB.57.12151.

Rtimi, M., Beydoun, N., Movsesyan, A., Akil, S., Kostcheev, S., Gassmann, X., Lajnef, M., Chtourou, R & Jradi, S. 2022. Enhanced Photocatalytic Activity and Photoluminescence of ZnO Nano-Wires Coupled with Aluminum Nanostructures. *Nanomaterials,* **12(11)**: 1941, https://doi.org/10.3390/nano12111941.

Subramani, A & Senthilnathan, T. 2019. Preparation, Characterization of Mg and Al co-doped ZnO nanoparticles and its application in congo red dye remediation. *Egyptian Journal of Chemistry*, **62 (Spl Issue 2)**: 617-625, https://doi.org/10.21608/ejchem.2019.15825.1957.

Tauc, J., Menth, A & Wood, D. L. 1970. Determination of optical band gap. *Physical Review Letters,* **25**: 749-752.

Welderfael, T., Pattabi, M., Pattabi, R. M & G, A. K. T. 2016. Photocatalytic activity of Ag-N co-doped ZnO nanorods under visible and solar light irradiations for MB degradation. *Journal of Water Process Engineering,* **14**: 117-123, https://doi.org/10.1016/j.jwpe.2016.11.001.

Welderfael, T., Yadav, O., Taddesse, A & Kaushal, J. 2013. Synthesis, characterization and photocatalytic activities of Ag-N-Codoped ZnO nanoparticles for degradation of

methyl red. *Bulletin of the Chemical Society of Ethiopia*, **27**, https://doi.org/10.4314/bcse.v27i2.7.

Yadav, S., Tiwari, K. S., Gupta, C., Tiwari, M. K., Khan, A & Sonkar, S. P. 2023. A brief review on natural dyes, pigments: Recent advances and future perspectives. *Results in Chemistry*, **5**: 100733, https://doi.org/10.1016/j.rechem.2022.100733.

Yung, K. C., Liem, H & Choy, H. S. 2009. Enhanced redshift of the optical band gap in Sn-doped ZnO free standing films using the sol–gel method. *Journal of Physics D: Applied Physics*, **42(18)**: 185002, https://doi.org/10.1088/0022-3727/42/18/185002.